https://doi.org/10.5194/egusphere-2026-4271
Preprint. Discussion started: 24 August 2026
© Author(s) 2026. CC BY 4.0 License.

Seasonal and regional sensitivities of secondary inorganic aerosols to NH_3 and NO_x emission reductions over China

Jiayu Xu[1], Alain Clappier[2*], Philippe Thunis[3], Xingpei Ye[4], Lu Li[1], and Lin Zhang[1*]

[1]Peking University, School of Physics, Department of Atmospheric and Oceanic Sciences, Beijing, China
[2]Université de Strasbourg, Laboratoire Image Ville Environnement, Strasbourg, France
[3]European Commission, Joint Research Centre (JRC), Ispra, Italy
[4]Jiangsu Guoxin Research Institute Co., Ltd., Nanjing, China

Correspondence to: Alain Clappier (alain.clappier@live-cnrs.unistra.fr) and Lin Zhang (zhanglg@pku.edu.cn)

Abstract. Secondary inorganic aerosols, comprising sulfate, nitrate, and ammonium (SNA), are major $PM_{2.5}$ pollution contributors in China, but the relative effectiveness of controlling their gaseous precursors (NH_3, NO_x, and SO_2) remains insufficiently quantified across seasons and regions. Here we use year-round WRF-Chem sensitivity simulations for 2017 to assess responses of surface SNA, population-weighted exposure, and $PM_{2.5}$-related premature mortality to independent 50% reductions in anthropogenic NH_3, NO_x, and SO_2 emissions over China. We find that NH_3 and NO_x reductions each decrease national mean SNA by 24–36% across seasons, whereas SO_2 reductions produce smaller decreases of 5–15%. NH_3 reduction is most effective in winter, decreasing national mean SNA by 32.7% (-3.88 μg m^{-3}), while NO_x reduction is more effective in spring and summer (up to -35.6%). Chemical-regime analysis using a potential impact indicator reveals that NH_3-sensitive regimes dominate more than 70% of China in winter, shifting to NO_x-sensitive regimes across eastern China in spring and summer, while SO_2-sensitive regimes appear mainly over the summertime arid west. Seasonal regime evolution shows a clear east–west contrast broadly aligned with the Hu Line. Halving either NH_3 or NO_x emissions could avert ~200,000 $PM_{2.5}$-related SNA-attributable premature deaths annually, with NO_x reductions offering larger national benefits and NH_3 reductions yielding greater benefits in several megacities. These results support seasonally and regionally differentiated NH_3 and NO_x control strategies for future $PM_{2.5}$ mitigation in China.

1 Introduction

Fine particulate matter ($PM_{2.5}$) pollution remains a major air quality challenge in China, with well-established consequences for human health and ecosystems. Reducing $PM_{2.5}$ is therefore a pivotal and continuing objective of China's environmental policy. One of the main challenges in designing efficient $PM_{2.5}$ control strategies lies in the complex, often nonlinear relationship between precursor emissions and pollutant concentrations. Source apportionment and sensitivity analysis are the two principal methodological approaches used to characterize these relationships (Clappier et al., 2017). Among $PM_{2.5}$ components, secondary inorganic aerosols, comprising sulfate (SO_4^{2-}), nitrate (NO_3^-), and ammonium (NH_4^+) (collectively referred to as SNA), are of particular importance, accounting for approximately 50% of $PM_{2.5}$ mass concentration in China on average (Lai et al., 2016; Liu et al., 2022b; Zhang et al., 2018). SNA formation is governed by three gaseous precursors, i.e., SO_2, NO_x, and NH_3, but the relative effectiveness of controlling these precursors varies with season, region, and precursor abundance. Identifying the dominant precursor sensitivity is therefore essential for designing targeted and efficient $PM_{2.5}$ control strategies.

Since the implementation of China's Air Pollution Prevention and Control Action Plan in 2013, SO_2 and NO_x emissions and ambient concentrations have declined substantially across eastern China (Vu et al., 2019; Zheng et al., 2018). As conventional end-of-pipe controls for SO_2 and NO_x approach their practical limits, additional reductions may become increasingly costly and may yield smaller marginal benefits. In contrast, agricultural NH_3 emissions have received less regulatory attention, while satellite observations indicate increasing atmospheric NH_3 concentrations over China (Lachatre et

https://doi.org/10.5194/egusphere-2026-4271
Preprint. Discussion started: 24 August 2026
© Author(s) 2026. CC BY 4.0 License.

al., 2019). Elevated NH_3 can sustain ammonium nitrate formation and weaken the $PM_{2.5}$ benefits of SO_2 and NO_x controls even as sulfate has substantially declined (Fu et al., 2017; Liu et al., 2021; Xu et al., 2019; Zhai et al., 2021). At the same time, a suite of agricultural management practices, including optimized nitrogen fertilizer application, deep fertilizer placement, low-protein livestock feed, and improved manure management, could reduce China's anthropogenic NH_3 emissions by 30–70% (Guo et al., 2020; Liu et al., 2019b; Xu et al., 2019; Zhang et al., 2020) while maintaining crop yields (Kang et al., 2023). A global cost-benefit analysis by Gu et al. (2021) revealed that the marginal abatement cost of NH_3 emissions is only approximately 10% of that for NO_x. These considerations make NH_3 abatement a potentially important component of future $PM_{2.5}$ mitigation strategies.

The effectiveness of NH_3 abatement, however, is neither spatially uniform nor independent of the concurrent trajectories of SO_2 and NO_x emissions. Previous modeling studies have shown that NH_3 reductions can effectively reduce $PM_{2.5}$, particularly the nitrate component, under present-day conditions in China (Erisman and Schaap, 2004; Xing et al., 2019; Xu et al., 2019; Zheng et al., 2019). For example, Li et al. (2021) found that NH_3 control is more effective than NO_x control for wintertime $PM_{2.5}$ and nitrate reduction in Beijing. Li et al. (2023) reached a similar conclusion for the effectiveness of NH_3 control on wintertime $PM_{2.5}$ in the Beijing-Tianjin-Hebei region during COVID-19 lockdown periods, while coordinated NO_x and volatile organic compounds (VOCs) reductions are more effective in southeastern coastal areas. However, the effectiveness of NH_3 abatement in reducing $PM_{2.5}$ over North China decreases as SO_2 and NO_x emissions decline (Liu et al., 2021), which is a trend that is expected as China's air quality policies continue to tighten. These findings indicate that the precursor-control effectiveness highly depends on season, region, and chemical background, and therefore cannot be generalized from individual regions or seasons.

Despite these advances, a systematic and spatially comprehensive assessment of the relative effectiveness of NH_3, NO_x and SO_2 controls across all of China and all seasons is still lacking. Existing studies have focused mainly on North China, individual city clusters, winter haze episodes, or annual-average conditions (Kang et al., 2023; Liu et al., 2021; Xu et al., 2019). This geographic and temporal fragmentation leaves several critical questions unresolved. First, how do SNA chemical regimes vary across China's diverse emission, meteorological, and chemical environments? Second, how do these regimes transition seasonally, and do they exhibit coherent national-scale spatial patterns? Third, to what extent do spatially differentiated precursor sensitivities translate into heterogeneous population exposure and health benefits? The health dimension is particularly important because the relationship between emission reductions and avoided premature mortality depends not only on the magnitude of concentration reductions but on their spatial overlap with population density (Liu et al., 2023a; Thunis et al., 2021), implying that the precursor that most effectively reduces SNA concentrations may not necessarily yield the greatest public health benefit.

To address these gaps, this study conducts year-round, nationwide sensitivity simulations using the WRF-Chem air quality model for 2017, and characterizes the responses of surface SNA concentrations to reductions in NH_3, NO_x, and SO_2 across all seasons and regions of China. Chemical regimes are analyzed using the potential impact (PI) indicator (Clappier et al., 2021), which provides a spatially resolved and directly comparable measure of each precursor's control over SNA formation. Public health implications are quantified through population-weighted concentration analysis and premature mortality estimation using the Global Exposure Mortality Model (GEMM). This study therefore provides a national-scale and seasonally resolved assessment of how NH_3, NO_x, and SO_2 controls affect SNA concentrations, chemical regimes, and health-relevant exposure, with implications for regionally differentiated $PM_{2.5}$ mitigation strategies in China.

https://doi.org/10.5194/egusphere-2026-4271
Preprint. Discussion started: 24 August 2026
© Author(s) 2026. CC BY 4.0 License.

2 Materials and methods

2.1 The WRF-Chem model

We use the Weather Research and Forecasting model coupled with Chemistry (WRF-Chem) version 3.6.1 to simulate the meteorological and atmospheric chemical fields for China from January to December in 2017. The single simulation domain covers all of China (Fig. S1) at a 27-km horizontal resolution. The 37 vertical layers extend from the surface to 50 hPa. The meteorological and chemical initial and lateral boundary conditions come from the Final (FNL) Operational Global Analysis data (NCEP, 2000) and the results of Community Atmosphere Model with Chemistry (CAM-Chem) (Buchholz et al., 2019) in 2017, respectively. We reinitialize the meteorological fields every 2 days to limit model drift (Zhou et al., 2021). For all scenarios, the 12 months are split into four quarterly simulations, with each simulation starting with a 3-day spin-up period. We update the model's static geographic information to the year 2017 using the Moderate Resolution Imaging Spectroradiometer (MODIS) Land Cover Type Product Version 6 (https://lpdaac.usgs.gov/products/mcd12q1v006/).

Atmospheric chemical processes are assessed using the Carbon-Bond Mechanism version Z (CBMZ) gas-phase chemical mechanism (Zaveri and Peters, 1999) coupled with a 4-bin sectional Model for Simulation Aerosol Interactions and Chemistry (MOSAIC-4 bins) aerosol scheme (Zaveri et al., 2008). Three heterogeneous reactions to form sulfate and nitrate on particle surfaces developed by Chen et al. (2016) are added to the MOSAIC scheme, which are detailed in Liu et al. (2021, 2023b), Xu et al. (2023) and Zhou et al. (2021). The shortwave and longwave radiation transfer scheme is the Rapid Radiative Transfer Model for GCMs (RRTMG) scheme (Iacono et al., 2008). Other physical parameterizations include the Yonsei University (YSU) planetary boundary layer scheme (Hong et al., 2006), the revised fifth-generation Mesoscale Model (MM5) Monin–Obukhov surface layer scheme (Chen and Dudhia, 2001) and the Unified Noah land-surface model (Niu et al., 2011), the Morrison 2-moment microphysics scheme (Morrison et al., 2009), and the Grell-3 cumulus scheme (Grell and Dévényi, 2002).

In the baseline simulation ("Base" case in Table 1), anthropogenic emissions over China are from 2017 Multi-resolution Emission Inventory for Climate and air pollution research-High Resolution (MEIC-HR) with a spatial resolution of 0.1° × 0.1°, and a monthly temporal resolution (Zheng et al., 2021). In particular, agricultural NH_3 emissions in 2017 were estimated using the upgraded methods of Chen et al. (2021), with the same temporal and spatial resolutions as the MEIC-HR inventory. In the rest of the domain, the 2010 monthly MIX emission inventory (Li et al., 2017) is used. Total emissions and monthly variations of each major pollutant in the MEIC-HR emission inventory are basically consistent with the commonly used MEIC emission inventory (with a spatial resolution of 0.25° × 0.25°), with the former being slightly higher in annual total emissions (Fig. S2). The annual total of the agricultural NH_3 emissions estimated in this study (9.84 Tg $year^{-1}$) is slightly lower than those in the MEIC emission inventory (10.27 Tg $year^{-1}$). The former provides higher emission estimates in March-July and lower estimates during the remaining months, which mainly reflects differences in the estimate of emissions related to fertilizer application. Biogenic and biomass burning emissions were calculated online within the model, combined with the Model of Emissions of Gases and Aerosols from Nature (MEGAN) (Guenther et al., 2006) and the high-resolution (1 km) Fire INventory from NCAR (FINN) (Wiedinmyer et al., 2011), respectively.

Table 1. Emission scenarios used in the WRF-Chem simulations for 2017.

Scenarios	Description
Base	Baseline emissions using MEIC-HR and updated agricultural NH_3 emissions over China.
r50NH3	Reduce the anthropogenic NH_3 emissions by 50% over China.
r50NOx	Reduce the anthropogenic NO_x emissions by 50% over China.
r50SO2	Reduce the anthropogenic SO_2 emissions by 50% over China.

https://doi.org/10.5194/egusphere-2026-4271
Preprint. Discussion started: 24 August 2026
© Author(s) 2026. CC BY 4.0 License.

Three sets of sensitivity simulations (Table 1) were conducted in this study to investigate the effects of anthropogenic NH_3, NO_x, and SO_2 emission reductions on the concentrations of secondary inorganic aerosols in China at the same level of abatement (50%). The 50% reduction level was selected because, at this magnitude, the emission–concentration relationship remains approximately linear in most cases for yearly averaged emission reductions, ensuring the robustness of the sensitivity analysis. Moreover, a 50% reduction in anthropogenic emissions represents an achievable target for China (Clappier et al. 2021). In particular, such a reduction in anthropogenic NO_x emissions could be realized through the large-scale deployment of clean energy alternatives and the implementation of nitrogen-reduction technologies across various industrial sectors, in line with China's carbon neutrality objectives (Yang et al., 2022; Zhao et al., 2013). In the agricultural sector, a 50% emission reduction target is likewise consistent with the anticipated mitigation potential and the strategic direction of national policies. As noted in the Introduction, a combination of agricultural management practices could reduce total anthropogenic NH_3 emissions in China by 30–70%.

2.2 Air pollutant measurements

Ground-based observations of NO_2, SO_2, NH_3, O_3, and $PM_{2.5}$, together with satellite retrievals of NH_3 are collected for model evaluation. Hourly observations of surface NO_2, SO_2, O_3, and $PM_{2.5}$ concentrations at 1614 sites across the country in 2017 are obtained from the China National Environmental Monitoring Centre (CNEMC, https://air.cnemc.cn:18007/). We further apply the station selection method proposed by Liu et al. (2018) to rule out stations with over 30% missing NO_2 data or gaps exceeding 72 hours per month (11% of total). The remaining 1214 stations (Fig. S1) then undergo data quality control for other pollutants, including outlier removal. Due to the systematic positive biases in NO_2 measurement caused by the interference of other oxidized nitrogen compounds (Lamsal et al., 2008; Zhang et al., 2016), the raw measured NO_2 concentrations are corrected by multiplying the monthly corrected factors (CF; Fig. S3) calculated following Lamsal et al. (2008). NO_2, alkyl nitrates (AN), peroxyacetyl nitrate (PAN), and HNO_3 concentrations used in this correction are obtained from the 2017 baseline GEOS-Chem High Performance simulations (Ye et al., 2024).

The ground-based observational data for NH_3 over China are sparse in 2017. Here, we collect weekly- or monthly-averaged NH_3 observations from 10 stations in North China (NC), 3 stations in the Yangtze River Delta area (YRD), and 1 station in the Sichuan Basin (SCB) (further details are provided in Table S1). These sites represent traffic, urban, rural, and background environments. To improve spatial coverage, daily NH_3 total columns from the Infrared Atmospheric Sounding Interferometer (IASI) on the Metop-A satellite (https://doi.org/10.25326/10) are further incorporated. The retrieval algorithm of NH_3 columns first calculates Hyperspectral Range Indices (HRIs), which represent the emission or absorption amplitude of NH_3 in the spectrum (Van Damme et al., 2014). HRIs are then converted into NH_3 columns using an improved neural network-based algorithm proposed by Whitburn et al. (2016) and further refined by Van Damme et al. (2017). This IASI/Metop-A NH_3 total column dataset has been validated in several studies (Heald et al., 2012; Liu et al., 2017; Van Damme et al., 2018), and shows good agreement with measurements of surface NH_3 concentrations in China (Liu et al., 2019a, 2022a). As this retrieval product does not require averaging kernels for comparison with model simulations (Whitburn et al., 2016), WRF-Chem NH_3 columns are calculated by vertically summing simulated NH_3 concentrations across all model layers.

2.3 Indicator of chemical regime

To compare the concentration responses to different precursor reductions in a consistent way, the potential impact (PI) indicator (Clappier et al., 2021) is employed in this study to determine the chemical regime of each grid cell. The definition of PI is as follows:

$$PI_{\alpha}^{prec} = \frac{\Delta C_{prec}^{\alpha}}{\alpha} \quad (1)$$

https://doi.org/10.5194/egusphere-2026-4271
Preprint. Discussion started: 24 August 2026
© Author(s) 2026. CC BY 4.0 License.

where *prec* represents the emission precursor (NH_3, NO_x, and SO_2); α is the fractional emission reduction, with 0 (1) denoting no (100%) emission reduction, and in this study α is 0.5 for all three precursors; ΔC is the difference in surface SNA concentrations between the emission reduction scenario and the baseline simulation. A PI value is calculated for each grid cell and precursor. When $PI_{0.5}^{NOx}$ of a grid is larger than its $PI_{0.5}^{NH3}$ and $PI_{0.5}^{SO2}$ (i.e., $PI_{0.5}^{NOx} > max\,(PI_{0.5}^{NH3}, PI_{0.5}^{SO2})$), it implies that the NO_x emission reduction has a larger impact on SNA concentrations than SO_2 and NH_3. Therefore, the SNA formation chemical regime of the grid cell is classified as NO_x-sensitive. The NH_3-sensitive or SO_2-sensitive chemical regimes are defined similarly.

In addition, this study defines March, April, and May (MAM) as spring months; June, July, and August (JJA) as summer months; September, October, and November (SON) as autumn months; December, January, and February (DJF) as winter months. January, April, July, and October are representative months for winter, spring, summer, and autumn, respectively. Seasonal means are calculated as arithmetic means of the three months in the season.

3 Results

3.1 Model evaluation

The comparisons of NO_2, maximum daily 8-hourly average (MDA8) O_3, SO_2, and $PM_{2.5}$ concentrations between the Base simulation and ground-based observations are shown in Fig. 1. The baseline simulation reproduces the main temporal variations and spatial patterns of these pollutants at the national scale in 2017. Simulated MDA8 O_3, SO_2 and $PM_{2.5}$ levels agree reasonably well with observations throughout the year (Fig. 1b–d), with annual mean biases of +5.5 μg m^{-3} (+5.8%), -1.7 μg m^{-3} (-9.6%), and -1.4 μg m^{-3} (-3.1%), respectively (Fig. 1f–h). Although simulated NO_2 levels are less satisfactory than the other pollutants (Fig. 1a), the simulated and observed time series for all pollutants, including NO_2, show high temporal correlation coefficients (Rs), mostly near or above 0.8 across seasons. The spatial Rs between annual mean simulations and observations generally exceed 0.5, with $PM_{2.5}$ and NO_2 above 0.7. These results indicate that the model reproduces the major features of air quality over China and provides a suitable basis for the sensitivity analyses below.

The model performance for NO_2 is less satisfactory than for O_3, SO_2, and $PM_{2.5}$ (Fig. 1a, e). As described in Sect. 2.2, the raw NO_2 observations contain systematic positive biases, hence are corrected by applying monthly CFs that are less than 1 (Fig. S3). This correction reduces the observed levels by 2.51, 3.91, 4.36, and 3.25 μg m^{-3} in winter, spring, summer, and autumn, respectively (Fig. 1a). Against these corrected observations, the model still underestimates surface NO_2 in all seasons, particularly in winter, spring, and autumn (Fig. 1a), with an annual mean underestimation of 6.9 μg m^{-3} (-23.5%; Fig. 1e). The simulation bias in summer is notably smaller, decreasing from 6.04 μg m^{-3} relative to raw observations to 1.68 μg m^{-3} after correction.

The remaining NO_2 underestimates may be attributed to the relatively low spatial resolution of the model compared to the point-based monitoring stations. By categorizing annual mean observed NO_2 concentrations into 5 μg m^{-3} intervals, and calculating the corresponding simulated NO_2 concentrations, we find that the discrepancy between the Base simulation and observations increases with higher NO_2 levels and the slope of discrepancy sharply rises at 50 μg m^{-3} (Fig. S4a), suggesting the limited ability of the model to reproduce high NO_2 concentrations. In addition, the observed surface NO_2 concentrations increased in parallel with corresponding population density and nighttime lighting indices with a distinct inflection point at 10 μg m^{-3} (Fig. S4b), implying a high correlation between surface NO_2 concentrations and human activities. We therefore infer that the stations with high observed NO_2 concentrations are typically located near line or point sources of high NO_x emissions, such as traffic arteries, factories, and power plants (Zhao et al., 2013). These sub-grid sources are not fully resolved at 27-km resolution, causing grid-cell mean concentrations to be lower than point observations, particularly in traffic- and industry-intensive cities such as Xi'an, Chengdu, and Guangzhou (Fig. 1e).

https://doi.org/10.5194/egusphere-2026-4271
Preprint. Discussion started: 24 August 2026
© Author(s) 2026. CC BY 4.0 License.

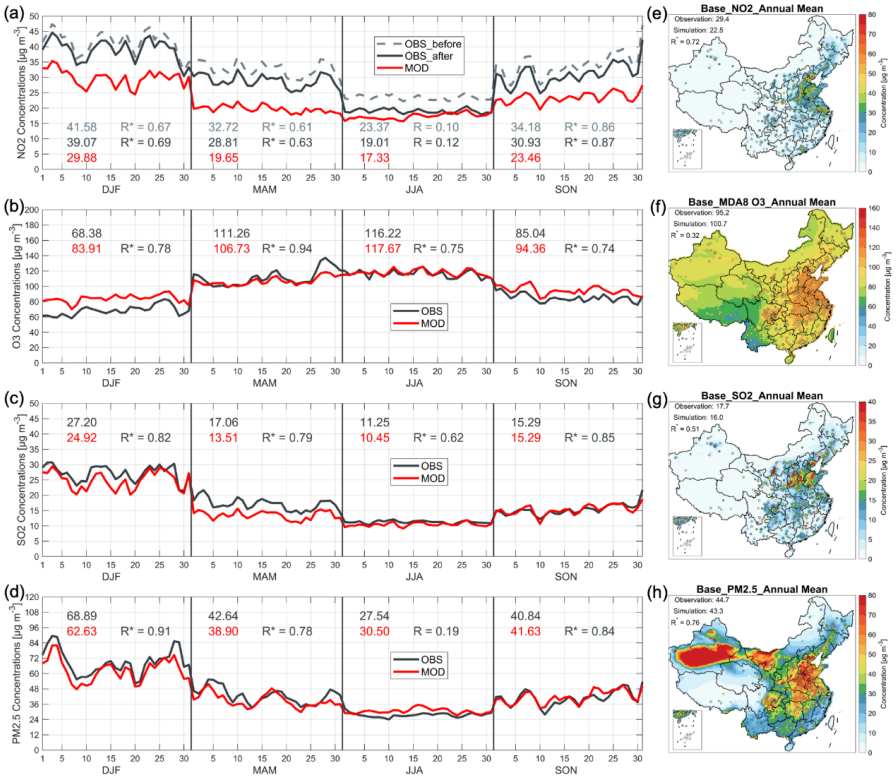

Figure 1. Evaluation of the WRF-Chem Base simulation against ground-based observations in 2017. The left column shows seasonally averaged daily variations of simulated (red) and observed (black) NO_2 (a), MDA8 O_3 (b), SO_2 (c), and $PM_{2.5}$ (d); the gray dashed line in (a) denotes raw NO_2 observations before correction; seasonal mean values are shown in the corresponding colors. The right column shows annual mean surface concentrations of each pollutant (e–h) for baseline simulation (contours) and observations (filled circles using the same color scale); annual mean values of all sites are shown inset. Temporal and spatial correlation coefficients (R) are shown inset; an asterisk indicates significance at the 95% confidence level.

We also evaluate baseline NH_3, an essential precursor of SNA, using IASI Metop-A satellite columns and the compiled surface measurements. The comparison results indicate that NH_3 simulated in the Base case generally agrees well with both satellite (Fig. 2) and surface observations (Fig. S5). Simulated monthly mean NH_3 columns in April, July, and October align well with IASI satellite observations in terms of magnitude and spatial distribution, with significant spatial Rs of 0.59, 0.79, and 0.44, respectively, and Reduced-Major-Axis (RMA) regression slopes close to 1 (Fig. 2). Similar agreement is found when comparing with ground-based observations at urban stations (Nanjing and Chengdu) in summer (Fig. S5c). However, simulated NH_3 levels in January are significantly lower than IASI observations (Fig. 2e, i), with a national mean bias of -7.1 μg m^{-3} (-82.5%) and a weak spatial R of only 0.15 (Fig. 2a).

Although IASI NH_3 retrievals have larger uncertainty in winter because of weak thermal contrast (Clarisse et al., 2009; Van Damme et al., 2017), the model also underestimates winter NH_3 compared with ground-based observations, particularly at urban stations where the largest bias reaches -11 μg m^{-3} (Fig. S5c). The collected winter surface NH_3 measurements are located in Beijing, Hebei, and Chengdu; among them, the Chengdu data align well with the 1:1 line (Fig. S5b). This suggests that the winter NH_3 underestimate is evident in North China, while its magnitude in the Sichuan Basin (SCB) remains less certain. For other seasons, the differences between baseline simulation and IASI NH_3 columns (Fig. 2e–h) suggest that the model biases

https://doi.org/10.5194/egusphere-2026-4271
Preprint. Discussion started: 24 August 2026
© Author(s) 2026. CC BY 4.0 License.

are generally larger in North China and SCB than in the Yangtze River Delta (YRD) and Pearl River Delta (PRD). More comprehensive surface NH_3 monitoring data are needed for a space-ground cross-validation across China.

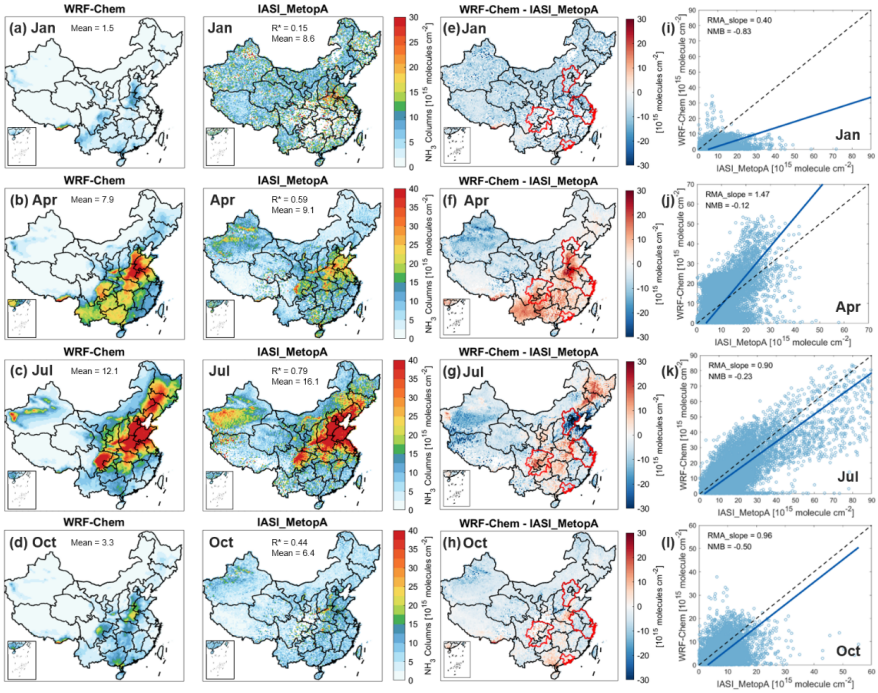

Figure 2. Spatial distributions of monthly mean NH_3 columns from the WRF-Chem Base simulation and IASI/Metop-A satellite observations in January, April, July, and October 2017. Panels (a–d) show simulated and observed NH_3 columns; panels (e–h) show model minus observation differences; panels (i–l) show the corresponding scatter plots. Values in (a–d) indicate national mean NH_3 columns and spatial correlation coefficients (R), with an asterisk denoting significance at the 95% confidence level. Red lines in panel (e) – (h) are the boundaries of Beijing-Tianjin-Hebei (BTH), Yangtze River Delta (YRD), Sichuan Basin (SCB), and Pearl River Delta (PRD) regions. Solid blue line, dashed black line, and NMB in panel (i) – (l) indicate Reduced-Major-Axis (RMA) regression, 1:1 line, and normalized mean bias, respectively.

3.2 Responses of absolute SNA concentrations to emission reductions

The year-round nationwide sensitivity simulations with equal fractional (50%) reductions in NH_3, NO_x, and SO_2 emissions provide a direct comparison of the effectiveness of these three precursors in reducing surface SNA concentrations. Figure 3 shows that 50% reductions in NH_3 or NO_x emissions lead to much larger decreases in SNA than an equivalent reduction in SO_2 emissions. Across the four representative months, national mean SNA decreases by 24–36% in the NH_3 and NO_x reduction scenarios, compared with only 5–15% in the SO_2 reduction scenario. This indicates that, under present-day Chinese conditions, SNA formation is primarily sensitive to NH_3 and NO_x controls, whereas the marginal effect of further SO_2 control is comparatively limited. The absolute SNA response is largest in regions with high baseline SNA concentrations, indicating that emission controls yield the greatest concentration benefits in existing pollution hotspots.

The relative effectiveness of NH_3 and NO_x reductions varies strongly by season. In January (representing winter), halving NH_3 emissions leads to a decrease of the national mean SNA concentration by 3.88 μg m^{-3} (-32.7%), which is greater than the effect of halving NO_x emissions (-2.87 μg m^{-3}, -24.2%). Spatially, the effects of these two precursor reductions on surface SNA are mainly concentrated in the SCB and Central China, including Hunan, Hubei, and Henan, with maximum reductions reaching 22 μg m^{-3}. Notably, NH_3 emission reduction has a broader spatial influence compared to NO_x, leading to SNA decreases of more than 10 μg m^{-3} across eastern (Anhui, Jiangsu, and Jiangxi), northern (Shaanxi, Shanxi, Shandong), and southwestern China (Guizhou and Guangxi).

https://doi.org/10.5194/egusphere-2026-4271
Preprint. Discussion started: 24 August 2026
© Author(s) 2026. CC BY 4.0 License.

In April (spring) and July (summer), NO_x reductions become more effective than NH_3 reductions in terms of both national mean response and spatial extent. The national mean SNA reduction from NO_x control reaches 35.6% in April and 31.0% in July, compared with 27.7% and 25.0% from NH_3 control, respectively. In spring, NO_x and NH_3 controls mainly reduce surface SNA across the transition zone between North, East, and Central China, while in summer their effects are more concentrated in North China, especially the BTH region and Shandong. In October (autumn), halving NH_3 emissions and halving NO_x emissions have comparable effects on the national mean (-2.9 μg m^{-3}, -33%) and maximum SNA concentrations (about -20 μg m^{-3}), but their spatial distributions differ. NO_x-related reductions extend from North China through East and Central China, whereas NH_3-related reductions are more concentrated over North China.

The four major urban agglomerations (BTH, SCB, YRD, and PRD) show additional regional differences (Fig. S6). In winter, SNA decreases least in the BTH region and most in the PRD under the NH_3 reduction scenario, with relative decreases of approximately 25% and 47%, respectively. This contrast is consistent with differences in atmospheric NH_3 abundance across regions (Fig. S7). The BTH region has higher excess NH_3 than the other urban agglomerations, which weakens the relative response of SNA to NH_3 reductions (Liu et al., 2021; Fig. S7). Overall, NH_3 and NO_x controls have comparable national importance for reducing SNA-related $PM_{2.5}$ in China, but their relative effectiveness varies strongly by season and region. NH_3 control is more effective in winter, while NO_x control has a greater impact in spring and summer. In autumn, both controls yield similar effects in North China, but NO_x reduction is more effective in Central China.

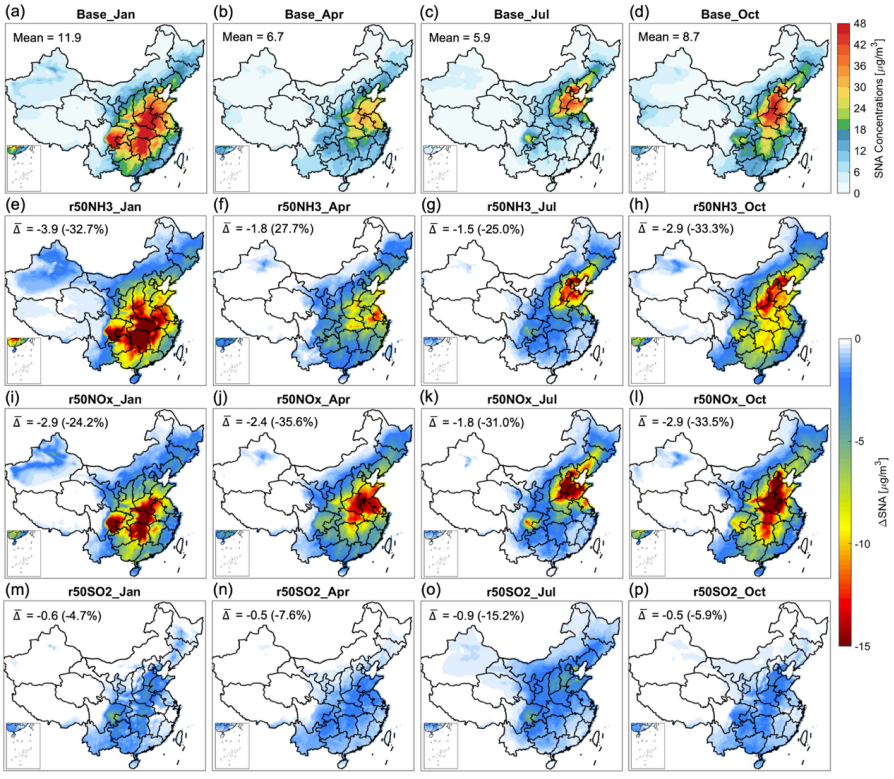

Figure 3. Monthly mean surface SNA concentrations (μg m^{-3}) over China in January, April, July, and October from the Base simulation (a–d), and differences with the r50NH3 (e–h), r50NOx (i–l), and r50SO2 (m–p) scenarios. Values inset are the national mean of each panel with percentages denoting relative changes to the Base simulation.

https://doi.org/10.5194/egusphere-2026-4271
Preprint. Discussion started: 24 August 2026
© Author(s) 2026. CC BY 4.0 License.

3.3 Responses of $PM_{2.5}$-related population exposure to emission reductions

To evaluate health-relevant exposure, this study further assesses the effect of precursor emission reductions on the population-weighted concentration (PWC) of SNA and associated premature mortality (estimated as the difference in $PM_{2.5}$-related mortality with and without the SNA following the GEMM framework, as detailed in Text S1). PWC assigns greater weight to pollutant concentrations in densely populated areas, providing a more accurate estimate of $PM_{2.5}$ exposure (Thunis et al., 2021). Most provinces show larger PWC than absolute SNA concentrations throughout the year (Fig. S8). The increments are particularly pronounced in Sichuan and Hebei, where both high SNA concentrations and dense population enhance exposure.

The precursor dependence of PWC reductions is broadly consistent with that of area-mean SNA reductions, but population weighting modifies the relative importance of NH_3 and NO_x controls in some regions. In January, most provinces show larger PWC reductions from NH_3 control, with the strongest decreases in Southwest and Central China (Fig. S8a). However, Sichuan and Henan show stronger PWC responses to NO_x reductions, even though their area-mean SNA responses to NH_3 and NO_x are similar. In April and July, NO_x reductions produce larger PWC decreases than NH_3 reductions in most provinces (Fig. S8b, c), with the largest decreases occurring in Anhui in spring (-13.0 μg m^{-3}) and Hebei in summer (-14.7 μg m^{-3}). An exception occurs in Beijing and Tianjin in summer, where PWC decreases are large and more responsive to NH_3 reductions than to NO_x reductions. In October, PWC reductions are generally smaller and more spatially heterogeneous. NO_x reductions dominate among provinces with larger PWC decreases, whereas NH_3 reductions are more influential in several provinces with smaller PWC responses. These results indicate that population weighting can alter the apparent priority of precursor controls, especially where concentration reductions overlap differently with population distribution.

The comparison between area-mean and population-weighted responses is also evident in the four urban agglomerations (Fig. S6). In the BTH region, NH_3 reductions produce larger SNA decreases in January, whereas NO_x reductions have stronger effects on PWC in the other representative months. In October, population weighting reverses the apparent control priority: NH_3 reductions are slightly more effective for area-mean SNA, but NO_x reductions become more effective for PWC. In the SCB, population weighting further highlights the importance of NO_x reductions across seasons. In the YRD and PRD, by contrast, population weighting has little effect on the relative importance of NH_3 and NO_x controls.

Table 2. Number of $PM_{2.5}$-related premature deaths attributable to SNA in Base scenario and avoided deaths under different precursor emission reductions.

Scenarios	$PM_{2.5}$-related premature deaths (thousand)	95% Confidence Interval
Base	649.6	[465.2, 832.1]
Base - r50NH3	190.0 (29%)	[177.7, 201.8]
Base - r50NOx	206.2 (32%)	[193.2, 218.7]
Base - r50SO2	45.3 (7%)	[42.4, 48.1]

Further investigation of health impacts shows that the baseline $PM_{2.5}$-related premature deaths attributable to SNA are estimated at 649,600 in 2017 (Table 2), mainly concentrated in densely populated urban agglomerations (Fig. 4a). The corresponding total $PM_{2.5}$-related premature mortality, computed directly from the full $PM_{2.5}$ field, is 2.17 million, consistent with previous estimates of 1.8 to 2.5 million for China (Burnett et al., 2018; Zhou et al., 2021). A 50% reduction in either NH_3 or NO_x emissions would avert around 200,000 $PM_{2.5}$-related SNA-attributable premature deaths annually in China (Table 2). NO_x reductions yield slightly larger national benefits (-206,200 deaths, -32%) than NH_3 reductions (-190,000 deaths, -29%), whereas SO_2 reductions prevent only about 45,300 deaths (7%) because of their smaller impact on SNA concentrations. The spatial patterns of avoided mortality differ between NH_3 and NO_x controls: NH_3 reductions provide larger benefits in

https://doi.org/10.5194/egusphere-2026-4271
Preprint. Discussion started: 24 August 2026
© Author(s) 2026. CC BY 4.0 License.

megacities such as Beijing, Shanghai, Guangzhou, and Shenzhen, whereas NO_x reductions provide larger benefits across Shandong, northern Jiangsu, Hebei, and broader interior regions (Fig. 4b–d).

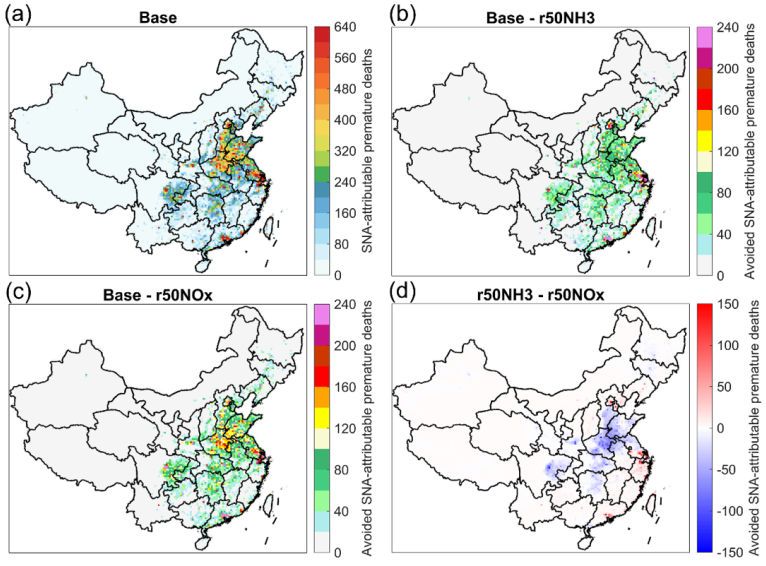

Figure 4. Annual $PM_{2.5}$-related premature deaths caused by SNA in Base scenario (a), avoided deaths due to 50% reductions in NH_3 (b) and NO_x (c) emissions, and the difference in avoided deaths between the NH_3 and NO_x reduction scenarios (d). Positive values in (d) indicate larger avoided mortality from NH_3 reduction than from NO_x reduction.

Among the four urban agglomerations, the YRD region shows the largest absolute mortality benefits from both NH_3 and NO_x controls, with approximately 39,300 and 37,400 avoided deaths, respectively (Fig. 5). This is largely attributable to the YRD's larger population of 238 million, compared with 110 million, 84 million, and 79 million in the BTH, SCB, and PRD regions, respectively (China Development Press, 2022; National Development and Reform Commission of China, 2025). The PRD region has the smallest absolute number of avoided deaths, below 8,000 for all three precursors, because of its smaller area and population, yet its relative reduction from NH_3 control reaches about 36%, the highest among four regions (Fig. 5). These results demonstrate that NH_3 and NO_x reductions both deliver substantial health benefits, but their relative importance differs across national totals, regional exposure, and urban-scale population distribution.

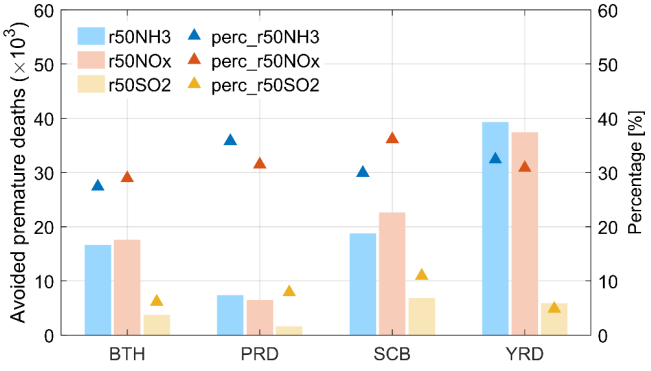

Figure 5. Number and percentage of avoided premature deaths in the BTH, PRD, SCB, and YRD regions under precursor emission reduction scenarios. Bars indicate the number of avoided deaths, and triangles indicate the percentage reduction relative to the baseline mortality.

https://doi.org/10.5194/egusphere-2026-4271
Preprint. Discussion started: 24 August 2026
© Author(s) 2026. CC BY 4.0 License.

3.4 SNA chemical regimes across China

For emission-control design, it is important not only to quantify the magnitude of SNA reductions but also to identify the precursor to which SNA formation is most sensitive in different regions and seasons. Here the chemical regime refers to the precursor whose 50% emission reduction produces the largest decrease in surface SNA concentration, as diagnosed by the PI indicator. The month-by-month maps and national areal fractions (Fig. 6 and Fig. 7) show a pronounced seasonal transition in SNA precursor sensitivity across China.

In winter (DJF), NH_3-sensitive regimes dominate most of China, accounting for more than 70% of the national model grids (Fig. 7). This pattern is consistent with low wintertime NH_3 emissions and relatively high NO_x emissions (Fig. S2), which consume much of the available NH_3 through neutralization of H_2SO_4 and HNO_3 and leave limited excess NH_3 (Fig. S7). In NH_3-poor regions like Zhejiang, western Inner Mongolia, and eastern Xinjiang, NH_3 availability is insufficient to fully neutralize HNO_3, so a 50% NH_3 reduction produces a larger SNA decrease than an equivalent NO_x reduction. By contrast, parts of Henan, Central China, and the Sichuan Basin (SCB) retain substantial excess NH_3 in winter (Fig. S7), and SNA formation there is more responsive to NO_x reductions.

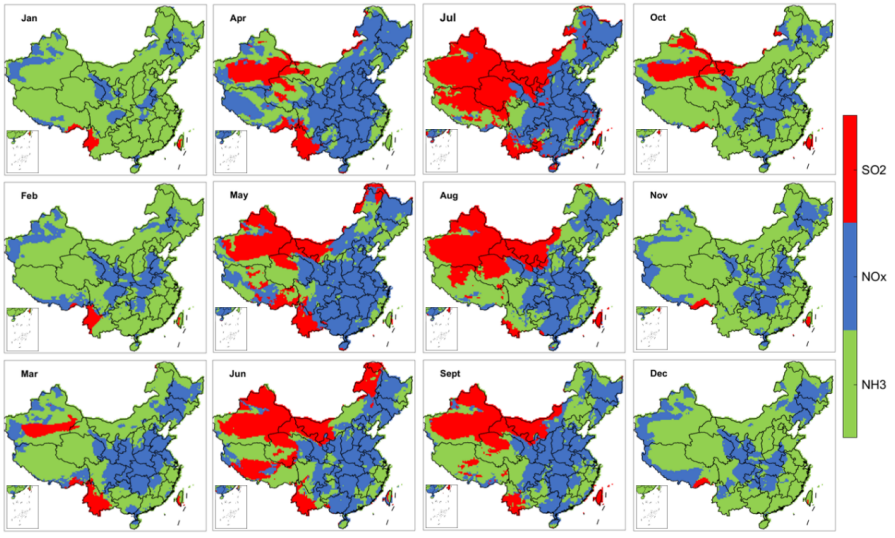

Figure 6. Monthly chemical regimes of surface SNA formation across China from January to December 2017. Green, blue, and red grid cells represent NH_3-, NO_x-, and SO_2-sensitive regimes, respectively, defined as the precursor whose 50% emission reduction produces the largest decrease in surface SNA concentration.

In spring (MAM), the dominant chemical regimes shift from NH_3- to NO_x-sensitive gradually. The fraction of NH_3-sensitive grid cells decreases from 58% in March to 26% in May (Fig. 7), while NO_x-sensitive regimes expand from Central China toward northeastern and southern China and reach their annual maximum areal fraction of 56% in April (Fig. 6). Nevertheless, several coastal or relatively NH_3-limited regions such as Liaoning, Zhejiang, Fujian, and Taiwan, remain more sensitive to NH_3 reductions (Fig. S7). In summer (JJA), NO_x-sensitive regimes persist over much of eastern China, whereas SO_2-sensitive regimes expand over the arid west, including desert and high-altitude regions in Xinjiang, Qinghai, Gansu, Inner Mongolia, and southwestern Yunnan. By July, SO_2-sensitive grids account for 42% of the national domain, slightly exceeding the NO_x-sensitive fraction (40%). From August onward, NH_3-sensitive regimes begin to re-expand, broadly mirroring their decline from winter to spring. The border region among Inner Mongolia, Heilongjiang, and Jilin remains consistently NO_x-sensitive during most months.

https://doi.org/10.5194/egusphere-2026-4271
Preprint. Discussion started: 24 August 2026
© Author(s) 2026. CC BY 4.0 License.

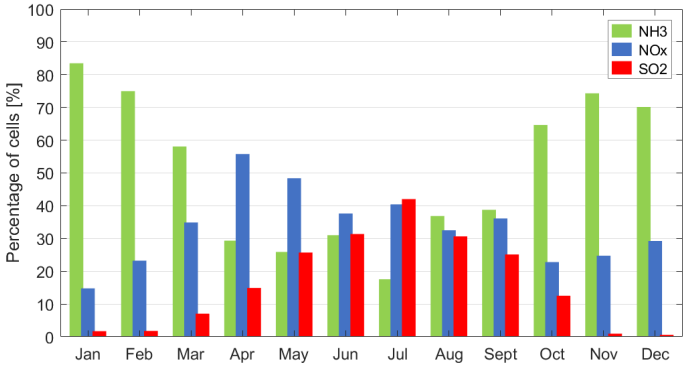

Figure 7. Monthly areal fractions of NH_3-, NO_x-, and SO_2-sensitive regimes across China in 2017. Fractions are calculated as the percentage of national model grid cells classified as sensitive to NH_3, NO_x, or SO_2 emissions based on the potential impact indicator.

To characterize the year-round behavior of each grid cell, we further classify the annual evolution of chemical regimes into seven categories: grids that are persistently sensitive to (1) NH_3, (2) NO_x, or (3) SO_2 emissions year-round, and grids that alternate between (4) NH_3-NO_x, (5) NH_3-SO_2, (6) NO_x-SO_2, and (7) NH_3-NO_x-SO_2 regimes during different months. The results in Fig. 8 reveal a coherent east–west contrast, which aligns closely with the Hu Line, i.e., the population density demarcation line. East of the Hu Line, where population and anthropogenic emissions are concentrated, most grids alternate between NH_3- and NO_x-sensitive regimes, constituting the largest category nationally (43%). West of the Hu Line, where SNA concentrations are generally lower and the environment is more arid, grids more often alternate among NH_3, SO_2, and NO_x sensitivity (27%) or between NH_3 and SO_2 sensitivity (23%). This spatial contrast indicates that the Hu Line is not only a demographic boundary but also a useful large-scale marker of contrasting precursor-sensitivity behavior for SNA formation.

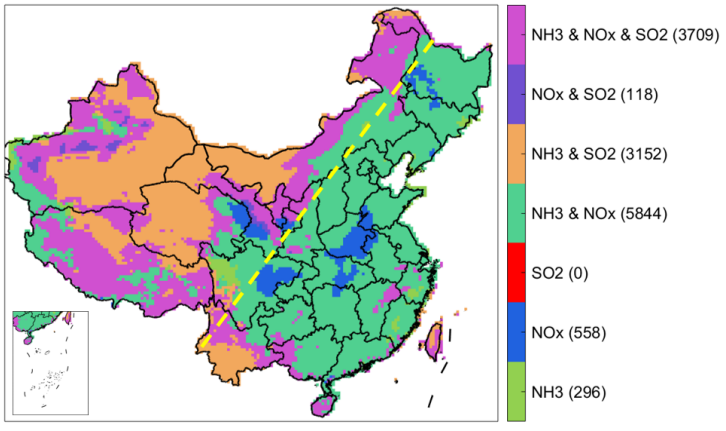

Figure 8. Annual variation patterns of chemical regimes for surface SNA formation across China. Colors denote grid cells that remain NH_3-, NO_x-, or SO_2-sensitive throughout the year, or that alternate among NH_3-NO_x, NH_3-SO_2, NO_x-SO_2, or NH_3-NO_x-SO_2 regimes during different months. The numbers in parentheses indicate the total number of grid cells in each category. The yellow dashed line denotes the Hu Line of population distribution.

Several subregions show persistent single-precursor sensitivity throughout the year. Year-round NO_x-sensitive regimes occur in parts of the SCB, eastern Henan, central Hubei, the Qinghai–Gansu border region, and southwestern Heilongjiang (Fig. 8), indicating that sustained NO_x reductions are particularly effective for SNA mitigation in these locations. The NO_x-sensitive pattern in the SCB is consistent with previous regional modeling results (Yang et al., 2022). In contrast, parts of

https://doi.org/10.5194/egusphere-2026-4271
Preprint. Discussion started: 24 August 2026
© Author(s) 2026. CC BY 4.0 License.

Fujian, Zhejiang, and western Sichuan remain NH_3-sensitive throughout the year, suggesting that continuous NH_3 reductions would provide the strongest SNA mitigation benefits there.

The regime maps in Fig. 8 identify the dominant precursor without indicating how strongly SNA responds to that precursor. To evaluate the sensitivity magnitude, we use the sensitivity coordinate system shown in Fig. S9 and plot provincial PI values for January, April, July, and October in Fig. 9. Provinces in NH_3- or NO_x-sensitive regimes generally lie farther from the origin and axes, indicating stronger and more distinguishable responses to NH_3 or NO_x reductions. In contrast, provinces classified as SO_2-sensitive usually remain close to the origin and axes, indicating weak absolute sensitivity and suggesting that SO_2-sensitive classifications should be interpreted cautiously, particularly where baseline SNA concentrations are low.

The provincial results reinforce the seasonal transition inferred from the grid-scale maps. In January, all provinces fall within the NH_3-sensitive quadrant, and most show strong NH_3 sensitivity, especially Shanxi, Anhui, and Hunan (Fig. 9a). All provinces also lie below the 1:1 line in the first quadrant, confirming the secondary role of NO_x reductions in winter. In April and July, most provinces shift to NO_x-sensitive regimes with relatively strong sensitivity (Fig. 9b, c), while a few provinces remain NH_3-sensitive, such as Fujian and Zhejiang in spring and Beijing and Tianjin in summer. These NH_3-sensitive provinces tend to lie close to the x-axis, implying that their sensitivity to NH_3 is only modestly stronger than their sensitivity to NO_x. In October, the number of NH_3-sensitive provinces increases again, with Shanxi and Henan showing the strongest sensitivities to NH_3 and NO_x reductions, respectively (Fig. 9d).

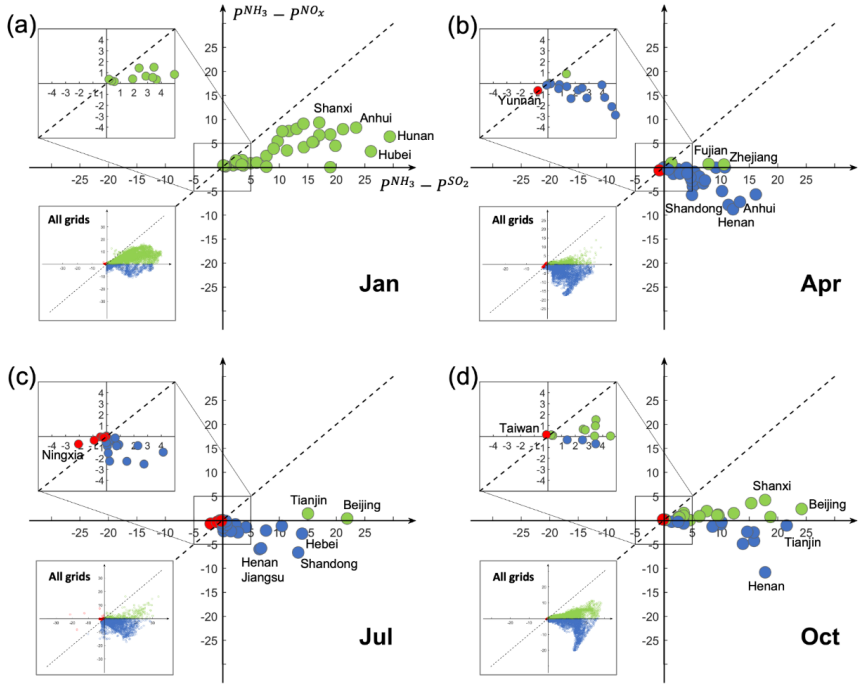

Figure 9. Provincial chemical regimes of SNA formation shown in the sensitivity coordinate system for January (a), April (b), July (c), and October (d). The inset in each panel shows the corresponding grid-cell results across China. Green, blue, and red markers indicate NH_3-, NO_x-, and SO_2-sensitive regimes, respectively. Greater distance from the origin and axes indicates stronger and more distinguishable sensitivity to the dominant precursor.

The four major urban agglomerations generally follow the national seasonal transition but with important regional differences (Fig. S10–S12). In the BTH, YRD, and PRD regions, more than 90% of grids alternate between NH_3- and NO_x-sensitive regimes over the year, with NH_3 sensitivity prevailing mainly in cold months and NO_x sensitivity in warm months.

https://doi.org/10.5194/egusphere-2026-4271
Preprint. Discussion started: 24 August 2026
© Author(s) 2026. CC BY 4.0 License.

This indicates that coordinated NH_3 and NO_x controls are needed, with the seasonal emphasis varying by region. In contrast, the Sichuan Basin contains a distinct area of persistent NO_x sensitivity in its northwestern part, covering much of Chengdu, and NO_x-sensitive regimes dominate more than half of the basin during most months except January. The YRD shows stronger NH_3 sensitivity in Zhejiang and Shanghai, while NO_x sensitivity expands from northern YRD toward the south in warm months. The PRD exhibits a rapid seasonal transition, with NH_3-sensitive regimes dominating from October to March and NO_x-sensitive regimes taking over from April onward. Patchy SO_2-sensitive grids appear in the YRD and PRD in July, but their low SNA concentrations and weak sensitivity suggest that NH_3 and NO_x remain the primary precursors of concern in these urban agglomerations.

The chemical-regime patterns in China share some similarities with those reported for Europe by Clappier et al. (2021), but also show important differences in spatial extent and relative dominance. In both regions, NH_3-sensitive regimes are most widespread in winter, SO_2-sensitive regimes expand in summer, and NO_x-sensitive regimes reach their largest extent in spring. However, the relative dominance of the three regimes differs substantially. SO_2-sensitive regimes are far less extensive in China (covering up to 40% of the territory in summer but dropping to less than 1% in winter) than in Europe (accounting for about 90% of the territory in July and still nearly 40% in winter). In contrast, NH_3-sensitive regimes remain more widespread in China (covering 70–80% of the territory in winter and remain 20–30% in summer) than in Europe (covering around 40% of the territory in winter and nearly absent in summer) throughout the year. NO_x-sensitive regimes are also more prominent in China, covering more than half of the national territory in April and remaining substantial during summer. These differences suggest that, under current Chinese conditions, future SNA mitigation requires continued NO_x reductions together with strengthened NH_3 controls, while the national marginal role of further SO_2 control is more limited and regionally confined.

4 Conclusions and discussion

This study uses year-round WRF-Chem sensitivity simulations for 2017 to quantify how surface secondary inorganic aerosols (SNA; sulfate, nitrate, and ammonium) over China respond to independent 50% reductions in anthropogenic NH_3, NO_x, and SO_2 emissions. We further diagnose SNA chemical regimes using the potential impact (PI) indicator and evaluate the exposure and health relevance of precursor controls using population-weighted concentrations and $PM_{2.5}$-related premature mortality estimates.

The results demonstrate that both NH_3 and NO_x controls are central to future SNA mitigation in China, whereas the marginal effect of further SO_2 control is comparatively limited under present-day conditions. At the national scale, 50% reductions in NH_3 and NO_x emissions decrease surface SNA concentrations by 24–36% across seasons, substantially larger than the 5–15% reduction from equivalent SO_2 control. The relative effectiveness of NH_3 and NO_x reductions varies strongly with season. NH_3 control is more effective in winter, reducing national mean SNA by 32.7%, while NO_x control becomes more effective in spring and summer, with the largest national decrease of 35.6% in April. In autumn, the national mean effects of NH_3 and NO_x controls are comparable, although their spatial patterns differ. These findings indicate that NH_3 and NO_x controls should not be viewed as substitutes, but as complementary measures whose relative priority depends on season and region.

The PI-based chemical-regime analysis provides a mechanistic interpretation of this seasonality. NH_3-sensitive regimes dominate more than 70% of China in winter, reflecting lower NH_3 emissions and stronger consumption of available NH_3 by acidic species. From spring to summer, NO_x-sensitive regimes expand across eastern China, while SO_2-sensitive regimes become more common over arid western regions where SNA concentrations and absolute sensitivities are generally low. The year-round evolution of chemical regimes reveals a clear east–west contrast broadly aligned with the Hu Line. East of the line, where anthropogenic emissions and population density are high, SNA formation is mainly characterized by seasonal alternation between NH_3- and NO_x-sensitive regimes. West of the line, chemical regimes more often alternate between NH_3 and SO_2

https://doi.org/10.5194/egusphere-2026-4271
Preprint. Discussion started: 24 August 2026
© Author(s) 2026. CC BY 4.0 License.

sensitivity or among all three precursors. Persistent single-precursor regimes are limited in spatial extent but are important for regional control strategies, including year-round NO_x sensitivity in parts of the Sichuan Basin, eastern Henan, and central Hubei, and year-round NH_3 sensitivity in parts of Fujian, Zhejiang, and western Sichuan.

By linking precursor sensitivity with population exposure, this study further shows that the health relevance of emission controls depends not only on concentration responses, but also on their spatial overlap with population. A 50% reduction in either NH_3 or NO_x emissions could avert around 200,000 $PM_{2.5}$-related premature deaths annually associated with SNA changes in China. NO_x reductions yield slightly larger national mortality benefits, while NH_3 reductions provide greater benefits in several densely populated megacities, including Beijing, Shanghai, Guangzhou, and Shenzhen. The comparison between concentration-based and population-weighted metrics also shows that the apparent priority of precursor control can change when population exposure is considered, underscoring the need to evaluate emission-control strategies using both air-quality and exposure-relevant indicators.

Several uncertainties should be considered when interpreting these results. First, the sensitivity simulations are based on a single reduction level of 50% for each precursor. Because SNA formation is chemically nonlinear, the relative benefits of NH_3, NO_x, and SO_2 controls may change at different abatement levels. Multi-level sensitivity simulations would be needed to identify thresholds, saturation effects, and marginal benefits along more realistic emission-reduction pathways. Second, each precursor is reduced independently in this study, whereas actual control policies usually change multiple pollutants simultaneously (Cheng et al., 2021; Geng et al., 2024). Combined reductions in NH_3, NO_x, SO_2, VOCs, primary particles, and carbon-related emissions may produce responses that differ from the sum of single-precursor effects because of nonlinear aerosol thermodynamics, oxidant chemistry, and nitrate formation. Third, the present analysis focuses on SNA-related $PM_{2.5}$ and does not fully resolve interactions between NO_x control, ozone chemistry, atmospheric oxidants, and secondary aerosol production. For example, NO_x reductions can increase ozone in VOC-limited environments by weakening NO titration, potentially enhancing oxidation pathways for nitrate or sulfate formation (Huang et al., 2021; Li et al., 2021). These feedbacks may partly offset direct SNA benefits in some regions and seasons.

Additional uncertainties arise from NH_3 emissions and health-impact estimation. The model underestimates NH_3 in winter, especially in North China, and previous studies have also suggested that urban NH_3 emissions may be substantially underestimated in Beijing (Xu et al., 2023). Such biases could affect the diagnosed NH_3 sensitivity and should be further constrained with expanded surface NH_3 measurements and satellite-based inversions. For health impacts, the mortality estimates should be interpreted as $PM_{2.5}$-related benefits associated with simulated SNA changes, rather than as a full accounting of total $PM_{2.5}$ responses, because changes in primary $PM_{2.5}$, organic aerosol, and other secondary components are not explicitly assessed here. Future work should calculate mortality directly from total simulated $PM_{2.5}$ responses when multi-component $PM_{2.5}$ changes are available.

Despite these uncertainties, the central implication is robust: future $PM_{2.5}$ mitigation in China requires coordinated NH_3 and NO_x controls with strong seasonal and regional differentiation. NH_3 abatement is particularly important in winter and in densely populated areas where exposure benefits are large, while NO_x control remains essential in warm seasons and in regions with persistent or recurrent NO_x-sensitive regimes. SO_2 control remains relevant in selected sulfur-sensitive regions, especially in western China, but its national marginal benefit for SNA mitigation is now smaller than that of NH_3 or NO_x. Overall, this study provides a spatially and seasonally resolved basis for incorporating NH_3 mitigation into China's next stage of $PM_{2.5}$ control, alongside continued NO_x reductions and region-specific multi-pollutant strategies.

https://doi.org/10.5194/egusphere-2026-4271
Preprint. Discussion started: 24 August 2026
© Author(s) 2026. CC BY 4.0 License.

Code and data availability

The WRF-Chem model output data of this study and the scripts developed for estimation and plotting are accessible upon reasonable request from the corresponding authors. The surface air quality monitoring data are publicly available from the China National Environmental Monitoring Centre (CNEMC) at https://air.cnemc.cn:18007/. The IASI/Metop-A NH_3 total column dataset is available at https://doi.org/10.25326/10. The MEIC-HR anthropogenic emission inventory data are available from the corresponding authors of Zheng et al. (2021) upon request.

Author contributions

JX, AC, and LZ conceived and designed the study. JX collected the data, conducted the model simulations, analyzed and visualized the results, and wrote the manuscript. AC developed the methodology and supervised the study. XY provided GEOS-Chem data for evaluation. PT and LL provided critical comments on the study. LZ acquired the funding and supervised the study. All authors reviewed and approved the final manuscript.

Competing interests

The authors declare that they have no conflict of interest.

Acknowledgements

The authors gratefully acknowledge the China National Environmental Monitoring Centre (CNEMC) for providing surface air quality monitoring data, the IASI/Metop-A NH_3 retrieval team for the satellite NH_3 total column dataset, and the Tsinghua University MEIC team for the MEIC-HR anthropogenic emission inventory.

Financial support

This work was supported by the National Key Research and Development Program of China (2023YFC3707404), the National Natural Science Foundation of China (41922037), and the High-performance Computing Platform of Peking University. JX acknowledges supporting from the China Scholarship Council.

References

Buchholz, R. R., Emmons, L. K., Tilmes, S., and The CESM2 Development Team: CESM2.1/CAM-chem Instantaneous Output for Boundary Conditions, https://doi.org/10.5065/NMP7-EP60, 2019.

Burnett, R., Chen, H., Szyszkowicz, M., Fann, N., Hubbell, B., Pope, C. A., Apte, J. S., Brauer, M., Cohen, A., Weichenthal, S., Coggins, J., Di, Q., Brunekreef, B., Frostad, J., Lim, S. S., Kan, H., Walker, K. D., Thurston, G. D., Hayes, R. B., Lim, C. C., Turner, M. C., Jerrett, M., Krewski, D., Gapstur, S. M., Diver, W. R., Ostro, B., Goldberg, D., Crouse, D. L., Martin, R. V., Peters, P., Pinault, L., Tjepkema, M., Van Donkelaar, A., Villeneuve, P. J., Miller, A. B., Yin, P., Zhou, M., Wang, L., Janssen, N. A. H., Marra, M., Atkinson, R. W., Tsang, H., Quoc Thach, T., Cannon, J. B., Allen, R. T., Hart, J. E., Laden, F., Cesaroni, G., Forastiere, F., Weinmayr, G., Jaensch, A., Nagel, G., Concin, H., and Spadaro, J. V.: Global estimates of mortality associated with long-term exposure to outdoor fine particulate matter, Proc. Natl. Acad. Sci. U.S.A., 115, 9592–9597, https://doi.org/10.1073/pnas.1803222115, 2018.

Chen, D., Liu, Z., Fast, J., and Ban, J.: Simulations of sulfate–nitrate–ammonium (SNA) aerosols during the extreme haze events over northern China in October 2014, Atmospheric Chemistry and Physics, 16, 10707–10724, https://doi.org/10.5194/acp-16-10707-2016, 2016.

https://doi.org/10.5194/egusphere-2026-4271
Preprint. Discussion started: 24 August 2026
© Author(s) 2026. CC BY 4.0 License.

Chen, F. and Dudhia, J.: Coupling an Advanced Land Surface–Hydrology Model with the Penn State–NCAR MM5 Modeling System. Part I: Model Implementation and Sensitivity, Monthly Weather Review, 129, 569–585, https://doi.org/10.1175/1520-0493(2001)129%3C0569:CAALSH%3E2.0.CO;2, 2001.

Chen, Y., Zhang, L., Henze, D. K., Zhao, Y., Lu, X., Winiwarter, W., Guo, Y., Liu, X., Wen, Z., Pan, Y., and Song, Y.: Interannual variation of reactive nitrogen emissions and their impacts on PM2.5 air pollution in China during 2005–2015, Environ. Res. Lett., 16, 125004, https://doi.org/10.1088/1748-9326/ac3695, 2021.

Cheng, J., Tong, D., Zhang, Q., Liu, Y., Lei, Y., Yan, G., Yan, L., Yu, S., Cui, R. Y., Clarke, L., Geng, G., Zheng, B., Zhang, X., Davis, S. J., and He, K.: Pathways of China's PM2.5 air quality 2015–2060 in the context of carbon neutrality, Natl Sci Rev, 8, nwab078, https://doi.org/10.1093/nsr/nwab078, 2021.

China Development Press: Characteristics, Problems, and Countermeasures of Population and Economic Distribution Changes in the Capital Metropolitan Area, China, 2022.

Clappier, A., Belis, C. A., Pernigotti, D., and Thunis, P.: Source apportionment and sensitivity analysis: two methodologies with two different purposes, Geosci. Model Dev., 10, 4245–4256, https://doi.org/10.5194/gmd-10-4245-2017, 2017.

Clappier, A., Thunis, P., Beekmann, M., Putaud, J. P., and De Meij, A.: Impact of SOx, NOx and NH3 emission reductions on PM2.5 concentrations across Europe: Hints for future measure development, Environment International, 156, 106699, https://doi.org/10.1016/j.envint.2021.106699, 2021.

Clarisse, L., Clerbaux, C., Dentener, F., Hurtmans, D., and Coheur, P.-F.: Global ammonia distribution derived from infrared satellite observations, Nature Geosci, 2, 479–483, https://doi.org/10.1038/ngeo551, 2009.

Erisman, J. W. and Schaap, M.: The need for ammonia abatement with respect to secondary PM reductions in Europe, Environmental Pollution, 129, 159–163, https://doi.org/10.1016/j.envpol.2003.08.042, 2004.

Fu, X., Wang, S., Xing, J., Zhang, X., Wang, T., and Hao, J.: Increasing Ammonia Concentrations Reduce the Effectiveness of Particle Pollution Control Achieved via SO_2 and NO_x Emissions Reduction in East China, Environ. Sci. Technol. Lett., 4, 221–227, https://doi.org/10.1021/acs.estlett.7b00143, 2017.

Geng, G., Liu, Y., Liu, Y., Liu, S., Cheng, J., Yan, L., Wu, N., Hu, H., Tong, D., Zheng, B., Yin, Z., He, K., and Zhang, Q.: Efficacy of China's clean air actions to tackle PM2.5 pollution between 2013 and 2020, Nat. Geosci., 17, 987–994, https://doi.org/10.1038/s41561-024-01540-z, 2024.

Grell, G. A. and Dévényi, D.: A generalized approach to parameterizing convection combining ensemble and data assimilation techniques, Geophysical Research Letters, 29, 38-1–38-4, https://doi.org/10.1029/2002GL015311, 2002.

Gu, B., Zhang, L., Van Dingenen, R., Vieno, M., Van Grinsven, H. J., Zhang, X., Zhang, S., Chen, Y., Wang, S., Ren, C., Rao, S., Holland, M., Winiwarter, W., Chen, D., Xu, J., and Sutton, M. A.: Abating ammonia is more cost-effective than nitrogen oxides for mitigating $PM_{2.5}$ air pollution, Science, 374, 758–762, https://doi.org/10.1126/science.abf8623, 2021.

Guenther, A., Karl, T., Harley, P., Wiedinmyer, C., Palmer, P. I., and Geron, C.: Estimates of global terrestrial isoprene emissions using MEGAN (Model of Emissions of Gases and Aerosols from Nature), Atmospheric Chemistry and Physics, 6, 3181–3210, https://doi.org/10.5194/acp-6-3181-2006, 2006.

Guo, Y., Chen, Y., Searchinger, T. D., Zhou, M., Pan, D., Yang, J., Wu, L., Cui, Z., Zhang, W., Zhang, F., Ma, L., Sun, Y., Zondlo, M. A., Zhang, L., and Mauzerall, D. L.: Air quality, nitrogen use efficiency and food security in China are improved by cost-effective agricultural nitrogen management, Nat Food, 1, 648–658, https://doi.org/10.1038/s43016-020-00162-z, 2020.

Heald, C. L., Collett, J. L., Lee, T., Benedict, K. B., Schwandner, F. M., Li, Y., Clarisse, L., Hurtmans, D. R., Van Damme, M., Clerbaux, C., Coheur, P.-F., Philip, S., Martin, R. V., and Pye, H. O. T.: Atmospheric ammonia and particulate inorganic nitrogen over the United States, Atmos. Chem. Phys., 12, 10295–10312, https://doi.org/10.5194/acp-12-10295-2012, 2012.

Hong, S.-Y., Noh, Y., and Dudhia, J.: A New Vertical Diffusion Package with an Explicit Treatment of Entrainment Processes, Monthly Weather Review, 134, 2318–2341, https://doi.org/10.1175/MWR3199.1, 2006.

Huang, X., Ding, A., Gao, J., Zheng, B., Zhou, D., Qi, X., Tang, R., Wang, J., Ren, C., Nie, W., Chi, X., Xu, Z., Chen, L., Li, Y., Che, F., Pang, N., Wang, H., Tong, D., Qin, W., Cheng, W., Liu, W., Fu, Q., Liu, B., Chai, F., Davis, S. J., Zhang, Q., and He, K.: Enhanced secondary pollution offset reduction of primary emissions during COVID-19 lockdown in China, Natl Sci Rev, 8, nwaa137, https://doi.org/10.1093/nsr/nwaa137, 2021.

https://doi.org/10.5194/egusphere-2026-4271
Preprint. Discussion started: 24 August 2026
© Author(s) 2026. CC BY 4.0 License.

Iacono, M. J., Delamere, J. S., Mlawer, E. J., Shephard, M. W., Clough, S. A., and Collins, W. D.: Radiative forcing by long-lived greenhouse gases: Calculations with the AER radiative transfer models, Journal of Geophysical Research: Atmospheres, 113, https://doi.org/10.1029/2008JD009944, 2008.

Kang, J., Wang, J., Heal, M. R., Goulding, K., de Vries, W., Zhao, Y., Feng, S., Zhang, X., Gu, B., Niu, X., Zhang, H., Liu, X., Cui, Z., Zhang, F., and Xu, W.: Ammonia mitigation campaign with smallholder farmers improves air quality while ensuring high cereal production, Nat Food, 4, 751–761, https://doi.org/10.1038/s43016-023-00833-7, 2023.

Lachatre, M., Fortems-Cheiney, A., Foret, G., Siour, G., Dufour, G., Clarisse, L., Clerbaux, C., Coheur, P.-F., Van Damme, M., and Beekmann, M.: The unintended consequence of SO2 and NO2 regulations over China: increase of ammonia levels and impact on PM2.5 concentrations, Atmos. Chem. Phys., 19, 6701–6716, https://doi.org/10.5194/acp-19-6701-2019, 2019.

Lai, S., Zhao, Y., Ding, A., Zhang, Y., Song, T., Zheng, J., Ho, K. F., Lee, S., and Zhong, L.: Characterization of PM2.5 and the major chemical components during a 1-year campaign in rural Guangzhou, Southern China, Atmos. Res., 167, 208–215, https://doi.org/10.1016/j.atmosres.2015.08.007, 2016.

Lamsal, L. N., Martin, R. V., van Donkelaar, A., Steinbacher, M., Celarier, E. A., Bucsela, E., Dunlea, E. J., and Pinto, J. P.: Ground-level nitrogen dioxide concentrations inferred from the satellite-borne Ozone Monitoring Instrument, Journal of Geophysical Research: Atmospheres, 113, https://doi.org/10.1029/2007JD009235, 2008.

Li, M., Zhang, Q., Kurokawa, J., Woo, J.-H., He, K., Lu, Z., Ohara, T., Song, Y., Streets, D. G., Carmichael, G. R., Cheng, Y., Hong, C., Huo, H., Jiang, X., Kang, S., Liu, F., Su, H., and Zheng, B.: MIX: a mosaic Asian anthropogenic emission inventory under the international collaboration framework of the MICS-Asia and HTAP, Atmos. Chem. Phys., 17, 935–963, https://doi.org/10.5194/acp-17-935-2017, 2017.

Li, M., Zhang, Z., Yao, Q., Wang, T., Xie, M., Li, S., Zhuang, B., and Han, Y.: Nonlinear responses of particulate nitrate to NO_x emission controls in the megalopolises of China, Atmospheric Chemistry and Physics, 21, 15135–15152, https://doi.org/10.5194/acp-21-15135-2021, 2021.

Li, R., Zhang, L., Gao, Y., and Wang, G.: Different Response Mechanisms of N-Bearing Components to Emission Reduction Across China During COVID-19 Lockdown Period, Journal of Geophysical Research: Atmospheres, 128, e2023JD039496, https://doi.org/10.1029/2023JD039496, 2023.

Liu, L., Zhang, X., Xu, W., Liu, X., Lu, X., Wang, S., Zhang, W., and Zhao, L.: Ground Ammonia Concentrations over China Derived from Satellite and Atmospheric Transport Modeling, Remote Sensing, 9, 467, https://doi.org/10.3390/rs9050467, 2017.

Liu, L., Zhang, X., Wong, A. Y. H., Xu, W., Liu, X., Li, Y., Mi, H., Lu, X., Zhao, L., Wang, Z., Wu, X., and Wei, J.: Estimating global surface ammonia concentrations inferred from satellite retrievals, Atmos. Chem. Phys., 19, 12051–12066, https://doi.org/10.5194/acp-19-12051-2019, 2019a.

Liu, M., Lin, J., Wang, Y., Sun, Y., Zheng, B., Shao, J., Chen, L., Zheng, Y., Chen, J., Fu, T.-M., Yan, Y., Zhang, Q., and Wu, Z.: Spatiotemporal variability of NO_2 and $PM_{2.5}$ over Eastern China: observational and model analyses with a novel statistical method, Atmospheric Chemistry and Physics, 18, 12933–12952, https://doi.org/10.5194/acp-18-12933-2018, 2018.

Liu, M., Huang, X., Song, Y., Tang, J., Cao, J., Zhang, X., Zhang, Q., Wang, S., Xu, T., Kang, L., Cai, X., Zhang, H., Yang, F., Wang, H., Yu, J. Z., Lau, A. K. H., He, L., Huang, X., Duan, L., Ding, A., Xue, L., Gao, J., Liu, B., and Zhu, T.: Ammonia emission control in China would mitigate haze pollution and nitrogen deposition, but worsen acid rain, Proc. Natl. Acad. Sci. U.S.A., 116, 7760–7765, https://doi.org/10.1073/pnas.1814880116, 2019b.

Liu, M., Lei, Y., Wang, X., Xue, W., Zhang, W., Jiang, H., Wang, J., and Bi, J.: Source Contributions to PM2.5-Related Mortality and Costs: Evidence for Emission Allocation and Compensation Strategies in China, Environ. Sci. Technol., 57, 4720–4731, https://doi.org/10.1021/acs.est.2c08306, 2023a.

Liu, P., Ding, J., Liu, L., Xu, W., and Liu, X.: Estimation of surface ammonia concentrations and emissions in China from the polar-orbiting Infrared Atmospheric Sounding Interferometer and the FY-4A Geostationary Interferometric Infrared Sounder, Atmos. Chem. Phys., 22, 9099–9110, https://doi.org/10.5194/acp-22-9099-2022, 2022a.

Liu, S., Geng, G., Xiao, Q., Zheng, Y., Liu, X., Cheng, J., and Zhang, Q.: Tracking Daily Concentrations of PM2.5 Chemical Composition in China since 2000, Environ. Sci. Technol., 56, 16517–16527, https://doi.org/10.1021/acs.est.2c06510, 2022b.

Liu, Z., Zhou, M., Chen, Y., Chen, D., Pan, Y., Song, T., Ji, D., Chen, Q., and Zhang, L.: The nonlinear response of fine particulate matter pollution to ammonia emission reductions in North China, Environ. Res. Lett., 16, https://doi.org/10.1088/1748-9326/abdf86, 2021.

https://doi.org/10.5194/egusphere-2026-4271
Preprint. Discussion started: 24 August 2026
© Author(s) 2026. CC BY 4.0 License.

Liu, Z., Rieder, H. E., Schmidt, C., Mayer, M., Guo, Y., Winiwarter, W., and Zhang, L.: Optimal reactive nitrogen control pathways identified for cost-effective PM2.5 mitigation in Europe, Nat Commun, 14, 4246, https://doi.org/10.1038/s41467-023-39900-9, 2023b.

Morrison, H., Thompson, G., and Tatarskii, V.: Impact of Cloud Microphysics on the Development of Trailing Stratiform Precipitation in a Simulated Squall Line: Comparison of One- and Two-Moment Schemes, Monthly Weather Review, 137, 991–1007, https://doi.org/10.1175/2008MWR2556.1, 2009.

National Development and Reform Commission of China: Leverage the comprehensive strengths of the Yangtze River Delta region, actively integrate into and serve the construction of the new development paradigm: https://www.ndrc.gov.cn/xwdt/ztzl/NEW_srxxgcjjpjjsx/yjcg/zw/202402/t20240208_1364056.html, last access: 6 March 2025.

NCEP: NCEP FNL Operational Model Global Tropospheric Analyses, continuing from July 1999 (updated daily), https://doi.org/10.5065/D6M043C6, 2000.

Niu, G.-Y., Yang, Z.-L., Mitchell, K. E., Chen, F., Ek, M. B., Barlage, M., Kumar, A., Manning, K., Niyogi, D., Rosero, E., Tewari, M., and Xia, Y.: The community Noah land surface model with multiparameterization options (Noah-MP): 1. Model description and evaluation with local-scale measurements, Journal of Geophysical Research: Atmospheres, 116, https://doi.org/10.1029/2010JD015139, 2011.

Thunis, P., Clappier, A., de Meij, A., Pisoni, E., Bessagnet, B., and Tarrason, L.: Why is the city's responsibility for its air pollution often underestimated? A focus on PM2.5, Atmospheric Chemistry and Physics, 21, 18195–18212, https://doi.org/10.5194/acp-21-18195-2021, 2021.

Van Damme, M., Clarisse, L., Heald, C. L., Hurtmans, D., Ngadi, Y., Clerbaux, C., Dolman, A. J., Erisman, J. W., and Coheur, P. F.: Global distributions, time series and error characterization of atmospheric ammonia (NH3) from IASI satellite observations, Atmos. Chem. Phys., 14, 2905–2922, https://doi.org/10.5194/acp-14-2905-2014, 2014.

Van Damme, M., Whitburn, S., Clarisse, L., Clerbaux, C., Hurtmans, D., and Coheur, P.-F.: Version 2 of the IASI NH3 neural network retrieval algorithm: near-real-time and reanalysed datasets, Atmos. Meas. Tech., 10, 4905–4914, https://doi.org/10.5194/amt-10-4905-2017, 2017.

Van Damme, M., Clarisse, L., Whitburn, S., Hadji-Lazaro, J., Hurtmans, D., Clerbaux, C., and Coheur, P.-F.: Industrial and agricultural ammonia point sources exposed, Nature, 564, 99–103, https://doi.org/10.1038/s41586-018-0747-1, 2018.

Vu, T. V., Shi, Z., Cheng, J., Zhang, Q., He, K., Wang, S., and Harrison, R. M.: Assessing the impact of clean air action on air quality trends in Beijing using a machine learning technique, Atmospheric Chemistry and Physics, 19, 11303–11314, https://doi.org/10.5194/acp-19-11303-2019, 2019.

Whitburn, S., Van Damme, M., Clarisse, L., Bauduin, S., Heald, C. L., Hadji-Lazaro, J., Hurtmans, D., Zondlo, M. A., Clerbaux, C., and Coheur, P. -F: A flexible and robust neural network IASI-NH3 retrieval algorithm, JGR Atmospheres, 121, 6581–6599, https://doi.org/10.1002/2016JD024828, 2016.

Wiedinmyer, C., Akagi, S. K., Yokelson, R. J., Emmons, L. K., Al-Saadi, J. A., Orlando, J. J., and Soja, A. J.: The Fire INventory from NCAR (FINN): a high-resolution global model to estimate the emissions from open burning, Geoscientific Model Development, 4, 625–641, https://doi.org/10.5194/gmd-4-625-2011, 2011.

Xing, J., Zhang, F., Zhou, Y., Wang, S., Ding, D., Jang, C., Zhu, Y., and Hao, J.: Least-cost control strategy optimization for air quality attainment of Beijing–Tianjin–Hebei region in China, Journal of Environmental Management, 245, 95–104, https://doi.org/10.1016/j.jenvman.2019.05.022, 2019.

Xu, J., Lu, M., Guo, Y., Zhang, L., Chen, Y., Liu, Z., Zhou, M., Lin, W., Pu, W., Ma, Z., Song, Y., Pan, Y., Liu, L., and Ji, D.: Summertime Urban Ammonia Emissions May Be Substantially Underestimated in Beijing, China, Environ. Sci. Technol., 57, 13124–13135, https://doi.org/10.1021/acs.est.3c05266, 2023.

Xu, Z., Liu, M., Zhang, M., Song, Y., Wang, S., Zhang, L., Xu, T., Wang, T., Yan, C., Zhou, T., Sun, Y., Pan, Y., Hu, M., Zheng, M., and Zhu, T.: High efficiency of livestock ammonia emission controls in alleviating particulate nitrate during a severe winter haze episode in northern China, Atmos. Chem. Phys., 19, 5605–5613, https://doi.org/10.5194/acp-19-5605-2019, 2019.

Yang, X., Lv, Y., Shao, P., Pan, Y., Fan, J., Wang, S., Zhang, X., Yi, J., Qiao, Y., and Wu, K.: Impacts of ammonia and nitrogen oxides emissions on fine particle matter pollution and mitigation potential over the Sichuan Basin, China Environmental Science, 42, 3502–3511, 2022.

https://doi.org/10.5194/egusphere-2026-4271
Preprint. Discussion started: 24 August 2026
© Author(s) 2026. CC BY 4.0 License.

Ye, X., Zhang, L., Wang, X., Lu, X., Jiang, Z., Lu, N., Li, D., and Xu, J.: Spatial and temporal variations of surface background ozone in China analyzed with the grid-stretching capability of GEOS-Chem High Performance, Science of The Total Environment, 914, 169909, https://doi.org/10.1016/j.scitotenv.2024.169909, 2024.

Zaveri, R. A. and Peters, L. K.: A new lumped structure photochemical mechanism for large-scale applications, Journal of Geophysical Research: Atmospheres, 104, 30387–30415, https://doi.org/10.1029/1999JD900876, 1999.

Zaveri, R. A., Easter, R. C., Fast, J. D., and Peters, L. K.: Model for Simulating Aerosol Interactions and Chemistry (MOSAIC), Journal of Geophysical Research: Atmospheres, 113, D13204, https://doi.org/10.1029/2007JD008782, 2008.

Zhai, S., Jacob, D. J., Wang, X., Liu, Z., Wen, T., Shah, V., Li, K., Moch, J. M., Bates, K. H., Song, S., Shen, L., Zhang, Y., Luo, G., Yu, F., Sun, Y., Wang, L., Qi, M., Tao, J., Gui, K., Xu, H., Zhang, Q., Zhao, T., Wang, Y., Lee, H. C., Choi, H., and Liao, H.: Control of particulate nitrate air pollution in China, Nat. Geosci., 14, 389–395, https://doi.org/10.1038/s41561-021-00726-z, 2021.

Zhang, L., Shao, J., Lu, X., Zhao, Y., Hu, Y., Henze, D. K., Liao, H., Gong, S., and Zhang, Q.: Sources and Processes Affecting Fine Particulate Matter Pollution over North China: An Adjoint Analysis of the Beijing APEC Period, Environ. Sci. Technol., 50, 8731–8740, https://doi.org/10.1021/acs.est.6b03010, 2016.

Zhang, X., Gu, B., Van Grinsven, H., Lam, S. K., Liang, X., Bai, M., and Chen, D.: Societal benefits of halving agricultural ammonia emissions in China far exceed the abatement costs, Nat Commun, 11, 4357, https://doi.org/10.1038/s41467-020-18196-z, 2020.

Zhang, Y., Lang, J., Cheng, S., Li, S., Zhou, Y., Chen, D., Zhang, H., and Wang, H.: Chemical composition and sources of PM1 and PM2.5 in Beijing in autumn, Science of The Total Environment, 630, 72–82, https://doi.org/10.1016/j.scitotenv.2018.02.151, 2018.

Zhao, B., Wang, S. X., Liu, H., Xu, J. Y., Fu, K., Klimont, Z., Hao, J. M., He, K. B., Cofala, J., and Amann, M.: NOx emissions in China: historical trends and future perspectives, Atmospheric Chemistry and Physics, 13, 9869–9897, https://doi.org/10.5194/acp-13-9869-2013, 2013.

Zheng, B., Tong, D., Li, M., Liu, F., Hong, C., Geng, G., Li, H., Li, X., Peng, L., Qi, J., Yan, L., Zhang, Y., Zhao, H., Zheng, Y., He, K., and Zhang, Q.: Trends in China's anthropogenic emissions since 2010 as the consequence of clean air actions, Atmos. Chem. Phys., 18, 14095–14111, https://doi.org/10.5194/acp-18-14095-2018, 2018.

Zheng, B., Cheng, J., Geng, G., Wang, X., Li, M., Shi, Q., Qi, J., Lei, Y., Zhang, Q., and He, K.: Mapping anthropogenic emissions in China at 1 km spatial resolution and its application in air quality modeling, Science Bulletin, 66, 612–620, https://doi.org/10.1016/j.scib.2020.12.008, 2021.

Zheng, M., Wang, Y., Bao, J., Yuan, L., Zheng, H., Yan, Y., Liu, D., Xie, M., and Kong, S.: Initial Cost Barrier of Ammonia Control in Central China, Geophys. Res. Lett., 46, 14175–14184, https://doi.org/10.1029/2019GL084351, 2019.

Zhou, M., Liu, H., Peng, L., Qin, Y., Chen, D., Zhang, L., and Mauzerall, D. L.: Environmental benefits and household costs of clean heating options in northern China, Nat Sustain, 5, 329–338, https://doi.org/10.1038/s41893-021-00837-w, 2021.